2020 IEEE PES Innovative Smart Grid Technologies Europe (ISGT-Europe)
Virtual, October 26-28, 2020

Supplementary Damping Control Design for Large Scale PV Power Plant at Transmission Level Interconnection

Younes J. Isbeih, Mohamed Shawky El Moursi
The Electrical Engineering and Computer Science Department
Khalifa University of Science and Technology
Abu Dhabi, United Arab Emirates
younes.isbeih, mohamed.elmoursi@ku.ac.ae

Mohamed Lotfi, Joao P. S. Catalao
Faculty of Engineering of the
University of Porto (FEUP) and INESC TEC
Porto, Portugal
mohd.f.lotfi@gmail.com, catalao@fe.up.pt

Mansour H. Abdel-Rahman
Department of Electrical Engineering, Electrical Engineering Department
The Czech Technical University, Mansoura University
Prague, The Czech Republic, Egypt
abdelman@fel.cvut.cz

***Abstract*—The deployment of large scale photovoltaic (PV) power generation has been witnessed in several countries worldwide with different installed capacities. Accordingly, codes and regulations to ensure secure and economical operation have been revised to address the challenges related with PV integration into electrical networks. This paper presents an H_∞ mixed sensitivity robust control design for enhancing the overall damping of low frequency oscillations. The presented architecture will implement the output signal of the power oscillator damper (POD) at the control loop of the PV-based solar power plant. The effectiveness of the proposed approach is tested using the New-England, 10-machines test system.**

***Index Terms*—H_∞ robust control techniques, low frequency power system oscillations, power oscillator damper (POD), PV power generation**

I. Introduction

THE small signal stability of a power system refers to its ability to maintain synchronism when it is subjected to a small disturbance. Consequently, the set of differential and algebraic equations (DAE) which describe the dynamic response of a power system can be linearized about an operating condition. In this context, the small-signal instability in practical power systems is associated with the insufficient damping of rotor oscillations which can grow in magnitude if sufficient damping torque is not provided [1]. Furthermore, the high penetration levels of renewable power generation can result in stressed operating conditions and thus reduce the overall damping of these oscillations if proper control schemes are not employed.

Two types of low-frequency power system oscillations are observed in large-interconnected power systems; local and inter-area modes. Local modes are triggered when synchronous machines oscillate against each other in one area at a frequency within the range of 1-2 Hz. On the other hand, the inter-area mode of oscillations can be observed over a large section of the network and involves one or group of generators swinging against a group of distinct generators. The frequency of such oscillations lies approximately within the range of 0.3-1 Hz [2]. To this end, the power system stabilizer (PSS) is developed to provide additional damping torque such that the oscillatory response is enhanced [3]. However, the design of PSSs is based on local measured signals and thus have limited impact on the damping of inter-area modes unless coordinated control is deployed [4].

Different supplementary control configurations and techniques are employed in the literature to improve the overall damping of power systems oscillations [5]–[12]. For example, a supplementary POD is designed to improve the damping of inter-area oscillations for large-scale PV using the minimax linear quadratic Gaussian-based control technique [5], [12]. The proposed approach is found to provide a robust damping performance over wide range of operating conditions and communication latency. However, limited damping levels can be obtained using this control technique since the cost function does not facilitate direct placement of the closed-loop poles to achieve the desired performance. A proportional integral derivative (PID) controller is implemented at the static var compensator (SVC) with integrated PV system to enhance transient stability [10].

Furthermore, a quasi-oppositional differential search algorithm is utilized to design the SVC-PID damping controller. Although the effectiveness of this approach is shown for the single machine infinite bus (SMIB) system, it is not tested on a practical multi-machine power system. On the other hand, a stability improvement approach is proposed for large-scale hybrid wind-photovoltaic (PV) power generation using an energy-storage unit based on supercapacitor (SC) [13]. The SC-based energy storage is connected to a common DC link through a bidirectional DC/DC converter to mitigate the power fluctuations due to the intermittent nature of solar irradiance and wind speed. Moreover, a PID-based supplementary damping controller is designed for the bidirectional DC/DC converter to improve the damping of low-

978-1-7281-7100-5/20/$31.00 ©2020 IEEE

frequency oscillations. Nevertheless, the practical limitations of the proposed configuration are not discussed as the large-scale 375 MW hybrid wind-PV farm is connected across a common DC-link.

The main contribution of this paper is to design a supplementary damping controller using reactive power modulation of the VSI of the PV power generation to enhance the overall damping of low-frequency power system oscillations. The control design is performed using H_∞ mixed sensitivity robust control techniques which allow the placement of the closed loop poles inside a pre-defined region for improved stability characteristics. The rest of the paper is organized as follows.The differential and algebraic equations (DAE) model of a power system is introduced in section II. Section III describes the mixed-sensitivity H_∞ robust control design in the LMI framework. In section IV, the effectiveness of the proposed approach is tested using the New-England, 10-machines system. Finally, conclusions are reported in section V.

II. The Mathematical Model of a Power System with PV Power Generation

The set of differential and algebraic equations (DAE) generally describe the dynamics the synchronous generators and its control systems, loads, the PV power plant in addition to the transmission network. In this paper, a fourth order model is used to describe the dynamics of synchronous generators [14]. In addition, they are equipped with static automatic voltage regulators (AVRs) as described in [15]. Moreover, a power system stabilizer (PSS) with two lead-lag compensators and washout filter is installed at some of the generators.

Fig.1 shows the single-diode equivalent circuit model of a PV cell [16]. This model can be extended to represented a PV array as per the method presented in [16]. As a result, the output current I_{PV} (A) of a PV array can be expressed as

$$I_{PV} = N_{mp}I_{ph} - N_{mp}I_0\left\{exp\left[\frac{q\,(V_{PV}+R_{sa}I_{PV})}{kATN_sN_{ms}}\right]-1\right\} - \frac{(V_{PV}+R_{sa}I_{PV})}{R_{pa}} \tag{1}$$

The detailed expressions are presented for the PV and reverse saturation currents (I_{ph}) and (I_0) [16]. The PV array is connected to the DC link through the DC/DC boost converter as shown in Fig.2. The mathematical equations which describe the dynamic average-value model of the DC/DC boost converter can be written as

$$C_p\frac{dV_{PV}}{dt} = I_{PV} - I_{LP} \tag{2}$$

$$L_p\frac{dI_{LP}}{dt} = V_{PV} - (1-D_P)V_{DC} - R_PI_{LP} \tag{3}$$

$$I_{PV_DC} = (1-D_P)I_{LP} \tag{4}$$

The DC/AC inverter is connected through an LC filter to Bus 13 which is considered as the point of common coupling

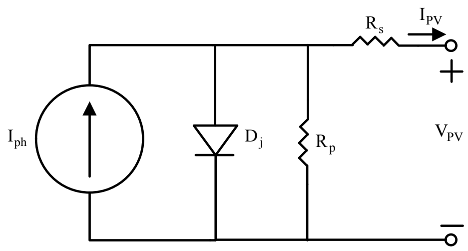

Fig. 1. Schematic diagram of single-diode equivalent-circuit model of the PV

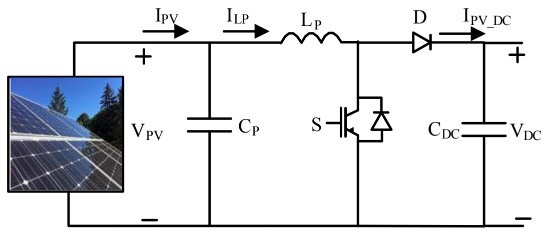

Fig. 2. Schematic diagram of the PV array and DC/DC boost converter

(PCC). The p.u. differential equations of the LC filter in a dq-reference frame can be written as

$$(L_I/\omega_b)\,\frac{di_{dI}}{dt} = -R_Ii_{dI} + \omega_eL_Ii_{qI} + v_{dI} - v_{dPCC} \tag{5}$$

$$(L_I/\omega_b)\,\frac{di_{qI}}{dt} = -R_Ii_{qI} - \omega_eL_Ii_{dI} + v_{qI} - v_{qPCC} \tag{6}$$

Fig. 3 shows the control block diagram of the DC/AC inverter. The main objective of the controller is to maintain a constant voltage (V_{DC}) across the DC-link at its reference value (V_{DC}^{ref}). It can also be noticed that the supplementary POD controller is implemented at the reactive power modulation of the VSI of the PV power plant. The measured input signal (Y_{meas}) should have high observability to inter-area modes of oscillations. The designed POD controller provides additional damping by producing a supplementary signal (V_s) as shown in Fig.3.

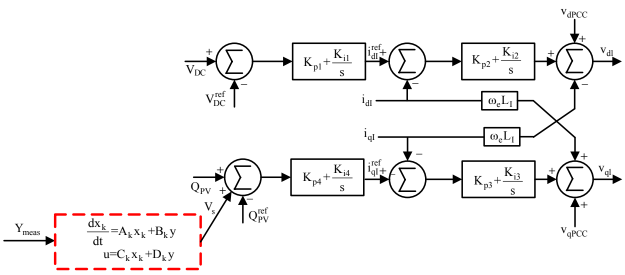

Fig. 3. Control block diagram of the VSI

III. Mixed-Sensitivity H_∞ Robust Control Design Using Linear Matrix Inequality (LMI) Approach

The linear model of a power system can be obtained by linearizing the nonlinear DAE model via Taylor series expansion about an equilibrium point [1]. The generalized form of the state-space realization of the power system can be written as follows

$$\Delta\dot{x} = A\Delta x + B\Delta u \quad (7)$$

$$\Delta y = C\Delta x + D\Delta u \quad (8)$$

where x,y and u are the state, algebraic and control input variables. The detailed linearized representation is not included in this paper due to space limitations. However, interested readers can find the complete derivation of the linear model in [14].

The linear model expressed in equations (7-8) is used to assess the small-signal stability of a power system by computing the eigenvalues of the system state matrix [1]. In addition, the overall damping of local and inter-area modes of oscillations can be found from the complex eigenvalues which occur in conjugate pairs. On the other hand, the derived model is employed to design the supplementary controller to enhance the overall damping of low-frequency inter-area oscillations as shown in Fig.3. The designed controller has to meet certain performance objectives such as disturbance rejection and measurement noise attenuation while maintaining the control efforts within the maximum limits of the VSI of the PV power plant. These control objectives are specified as constraints on the closed loop transfer functions such as the sensitivity S and/or complementary sensitivity functions T which are defined as follows

$$S = (I + GK)^{-1} \quad (9)$$

$$T = GK(I + GK)^{-1} = I - S \quad (10)$$

where G and K correspond to the open loop transfer function of the power system and the supplementary POD controller.

The output sensitivity function S should be made small for specific ranges of frequencies in order to mitigate the impact of the disturbance d on the output y. In this context, frequency-dependent singular values can be used to directly reflect this objective. For example, disturbance rejection and good command tracking requires that $\bar{\sigma}(S) \leq 1$ over the low frequency range.

Appropriatly selected weigting functions can better reflect the control performance objectives. For example, the designed controller should minimize the maximum gain of the weighed closed loop transfer functions W_1S and W_2KS over all frequencies. The maximum gain of a transfer function over all frequencies is known as the H_∞ norm. Consequently, the suboptimal control problem may be formulated as finding all the stabilizing controllers K such as that H_∞ norm of the weighted mixed sensitivity transfer functions is less than or equal γ, where γ is the bound on the H_∞ norm [17]. This can be written as:

$$\left\| \begin{matrix} W_1S \\ W_2KS \end{matrix} \right\|_\infty \leq \gamma \quad (11)$$

where the controller K can also be expressed in state space representation as:

$$\dot{x}_k = A_k x_k + B_k y \quad (12)$$

$$u = C_k x_k + D_k y \quad (13)$$

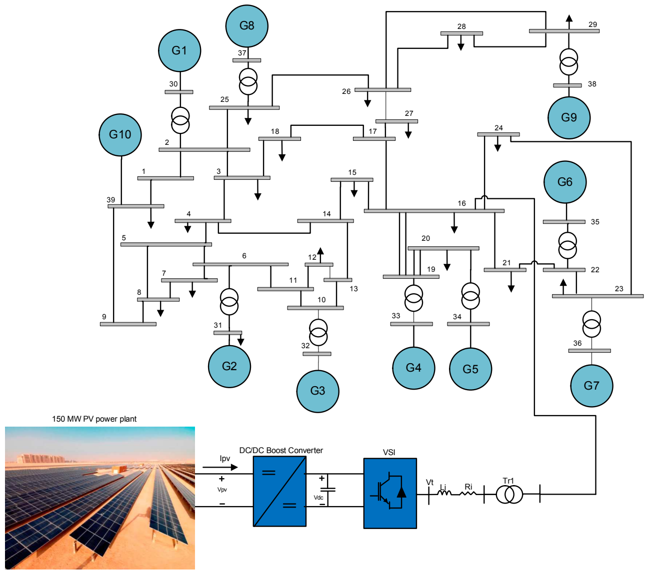

Fig. 4. Revised New England 39-bus system

As mentioned previously, an internally stabilizing controller is to be computed to minimize the weighted closed loop transfer functions as expressed in (11). The solution to this probelm can be found by solving two algebraic riccati equations either analytically as described in [17] or numerically using the LMI approach. The later one is used to synthesis the controller since it facilitates the placement of the closed loop poles in a pre-defined LMI region. The control design objective described previously is met if there exists an $X = X^T > 0$ such that

$$\begin{pmatrix} A_{cl}^T X + X + A_{cl} & B_{cl} & X C_{cl}^T \\ B_{cl}^T & -I & D_{cl}^T \\ C_{cl} X & D_{cl} & -\gamma^2 I \end{pmatrix} < 0 \quad (14)$$

with $\|T_{zw}\|_\infty < \gamma$. The LMI formulation facilitates also the placement of closed loop poles inside a pre-defined region which is assumed to be a conic sector. A minimum damping ratio of $\zeta = cos(\frac{\theta}{2})$ is guaranteed for all the poles which lie inside this region if and only if there exists $X = X^T > 0$ such that the following matrix inequality is satisfied [18]

$$\begin{pmatrix} sin\theta(A_{cl}X + XA_{cl}^T) & cos\theta(A_{cl}X - XA_{cl}^T) \\ cos\theta(XA_{cl}^T - A_{cl}X) & sin\theta(XA_{cl}^T + A_{cl}X) \end{pmatrix} < 0 \quad (15)$$

IV. Case Study: The New-England 39-Bus System

Fig.4 presents the revised 10 machines, 39-bus New England system with large scale PV power generation. The synchronous generators $G_{1,2,3,9}$ are only equipped with PSS. The parameters of this system are directly taken from [15]. A 150 MW solar PV power plant is installed at bus 16 and is formed by aggregating 300 $\times$ 0.5 MW PV arrays which parameters are given in [9].

A. Modal Analysis and Damping Control Design

The nonlinear model of the previously described system is built in MATLAB/Simullink. The modal analysis is carried

TABLE I
OSCILLATION MODES AND DAMPING RATIOS WITH PV AT SOLAR IRRADIANCE OF 1000 W/m^2

Mode	Eigenvalues without PV	Eigenvalues with PV without POD	Eigenvalues with PV with POD
1^{st}	$-1.8445 \pm j9.9134$ ($\zeta = 18.29\%, f = 1.58Hz$)	$-1.8407 \pm j9.9064$ ($\zeta = 18.27\%, f = 1.58Hz$)	$-1.8086 \pm j8.5014$ ($\zeta = 20.81\%, f = 1.35Hz$)
2^{nd}	$-0.4444 \pm j8.8254$ ($\zeta = 5.03\%, f = 1.40Hz$)	$-0.4450 \pm j8.8238$ ($\zeta = 5.04\%, f = 1.40Hz$)	$-0.6273 \pm j8.8210$ ($\zeta = 7.09\%, f = 1.40Hz$)
3^{rd}	$-0.6972 \pm j8.7909$ ($\zeta = 7.91\%, f = 1.40Hz$)	$-0.6996 \pm j8.7949$ ($\zeta = 8.82\%, f = 1.40Hz$)	$-0.3099 \pm j8.6230$ ($\zeta = 3.59\%, f = 1.37Hz$)
4^{th}	$-1.6164 \pm j8.5534$ ($\zeta = 18.57\%, f = 1.36Hz$)	$-1.6709 \pm j8.4435$ ($\zeta = 19.41\%, f = 1.34Hz$)	$-0.4399 \pm j8.8234$ ($\zeta = 4.98\%, f = 1.40Hz$)
5^{th}	$-2.1418 \pm j7.2821$ ($\zeta = 28.22\%, f = 1.16Hz$)	$-2.1410 \pm j7.2713$ ($\zeta = 28.45\%, f = 1.16Hz$)	$-1.6945 \pm j7.8972$ ($\zeta = 20.98\%, f = 1.26Hz$)
6^{th}	$-1.1574 \pm j7.3081$ ($\zeta = 15.64\%, f = 1.16Hz$)	$-1.0386 \pm j7.1894$ ($\zeta = 14.30\%, f = 1.14Hz$)	$-0.3625 \pm j7.1210$ ($\zeta = 5.08\%, f = 1.13Hz$)
7^{th}	$-0.5267 \pm j6.9417$ ($\zeta = 7.56\%, f = 1.10Hz$)	$-0.5209 \pm j6.8755$ ($\zeta = 7.56\%, f = 1.09Hz$)	$-1.2207 \pm j7.1226$ ($\zeta = 16.89\%, f = 1.13Hz$)
8^{th}	$-0.5015 \pm j6.3303$ ($\zeta = 7.90\%, f = 1.01Hz$)	$-0.5119 \pm j6.3146$ ($\zeta = 8.08\%, f = 1.01Hz$)	$-0.5259 \pm j6.0069$ ($\zeta = 8.72\%, f = 0.96Hz$)
9^{th}	$-0.3275 \pm j3.9344$ ($\zeta = 8.30\%, f = 0.63Hz$)	$-0.2735 \pm j3.9202$ ($\zeta = 6.96\%, f = 0.62Hz$)	$-1.2562 \pm j4.9437$ ($\zeta = 24.63\%, f = 0.79Hz$)
10^{th}			$-1.1416 \pm j4.0432$ ($\zeta = 27.17\%, f = 0.64Hz$)

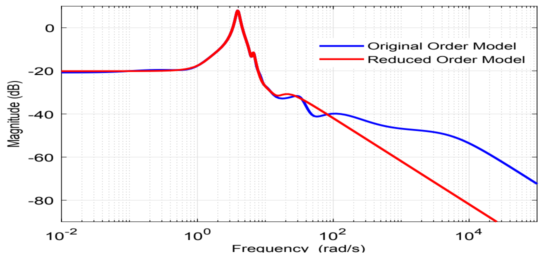

Fig. 5. The Original and reduced order model

out after linearising the nonlinear model about the nominal operating condition. The order of the obtained linear model is 114. Table I lists the eigenvalues of the linear model, that corresponds to all oscillatory modes along with their damping ratios (ζ) and frequencies with and without the PV power generation. It is noticed that the damping ratio of the 9^{th} mode which corresponds to an inter-area one is below 10% if PV power generation is not integrated. This scenario is worsened when the PV power plant is installed at bus 16 as the damping ratio decreases to 6.96%. As a result, a supplementary damping controller is required to enhance the damping of this mode as will be shown in the next section.

The order of the supplementary damping controller which is found using H_∞ norm minimization techniques equals the order of the open-loop system and the weighting functions. As a result, it is mandatory to reduce the order of the original model to simplify the design procedure and to avoid complexity in the synthesized controller. In this context, balanced truncation is employed to reduce the order of the original model. The main objective is to maintain a good approximation in the frequency rang e (0.1-3) Hz. A tenth-order model is found to exhibit a good approximate to the original model as shown in Fig. 5. A conic sector with inner angle $\theta = 2cos^{-1}(0.2) = 156.9261^\circ$ and apex at the origin is used for pole placement. In addition, the weighting functions W_1 and W_2 are found to satisfy the desired control objectives

$$W_1 = \frac{0.6095s^2 + 15.11s + 93.67}{s^2 + 5.074s + 6.437}, W_2 = 0.1 \quad (16)$$

The built-in MATLAB function $hinfmix$ is used to solve the general H_∞ weighted function mixed-sensitivity problem

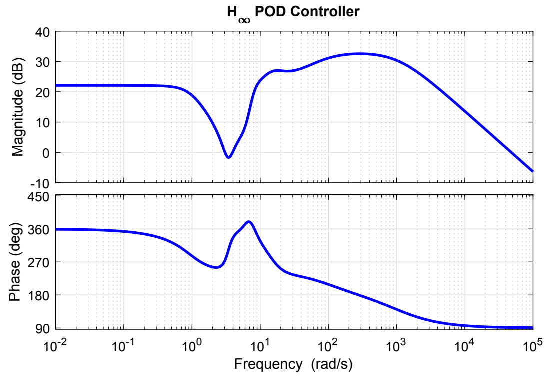

Fig. 6. The frequency response of the designed POD controller

using the LMI framework. The achieved H_∞-norm of the synthesized controller is found to be 8.08. Fig. 6 shows the frequency response of the designed POD controller which is also expressed in 17.

$$K_{POD}^{PV} = \frac{N(s)}{D(s)} \quad (17)$$

where

$$\begin{aligned} N(s) &= -48034(s+17.59)(s+4.18)(s^2+2.47s+2.32) \\ &\quad \times (s-5.35)(s^2+1.21s+11.55)(s^2+3.07s+38.29) \\ &\quad \times (s^2+33.65s+388.5) \\ D(s) &= (s+1055)(s+83.7)(s+17.53)(s+4.1)(s+2.55) \\ &\quad \times (s+2.52)(s^2+1.43s+1.01)(s^2+4.07s+63.93) \\ &\quad \times (s^2+14.42s+224.6) \end{aligned}$$

Table I presents the eigenvalues, damping ratios and frequencies which correspond to low-frequency power system oscillations for the closed-loop system with the designed POD controller. It can be clearly noticed that the overall damping of inter-area modes are considerably enhanced. For example, the damping ratio of the 9^{th} mode has increased from 8.30% to 27.17%. Furthermore, this is evident from the dynamic response of the test system which is shown in Figs.7,8,9 and 10. A three-phase-to-ground fault is applied at bus 28 at $t = 1$s and is naturally cleared after 100 ms. When the supplementary POD controller is implemented at the reactive power modulation of the PV-VSI, the overall damping of the system is considerably enhanced as the oscillations decay before 10 s.

V. CONCLUSION

The presence of poorly damped low-frequency power system oscillations constrain the amount of power transfer across the transmission network. In this paper, a supplementary damping control is designed for large-scale PV power plant using the weighted function mixed-sensitivity H_∞ robust control technique. The presented modal analysis and time-domain simulation successfully demonstrate the ability of PV power plant to enhance the overall damping of power system oscillations.

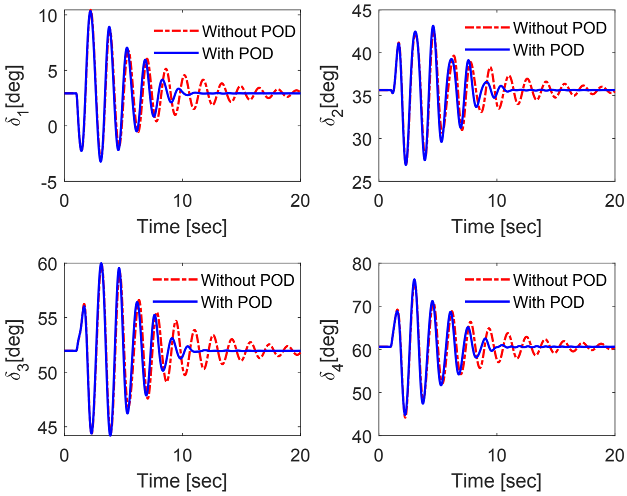

Fig. 7. Relative rotor angle positions of generators G_{1-4}

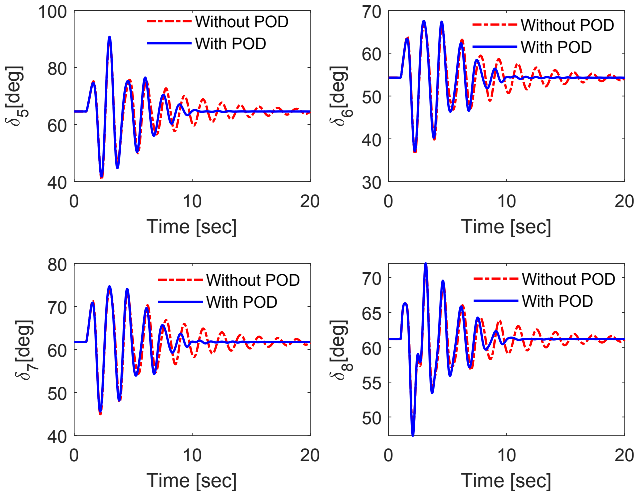

Fig. 8. Relative rotor angle positions of generators G_{5-8}

ACKNOWLEDGMENT

This paper is based upon work supported by the Khalifa University of Science and Technology under Award No. [CIRA-2018-37].

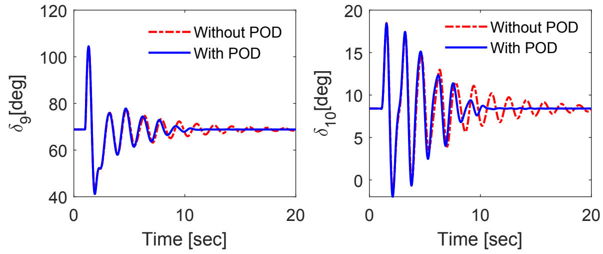

Fig. 9. Relative rotor angle positions of generators G_{9-10}

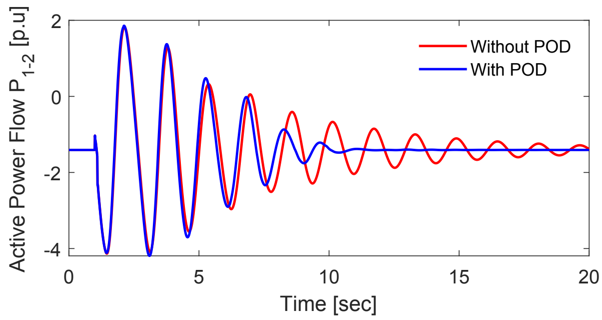

Fig. 10. Dynamic response of the active power flow P_{1-2}

REFERENCES

[1] P. Kundur, N. J. Balu, and M. G. Lauby, *Power system stability and control*. McGraw-hill New York, 1994, vol. 7.

[2] B. Pal and B. Chaudhuri, *Robust control in power systems*. Springer Science & Business Media, 2006.

[3] S. Ghosh, Y. Isbeih, M. S. El Moursi, and E. El-Saadany, "Cross-gramian model reduction approach for tuning power system stabilizers in large power networks," *IEEE Transactions on Power Systems*, 2019.

[4] Y. Isbeih, M. El Moursi, W. Xiao, and E. F. El-Saadany, "H mixed sensitivity robust control design for damping low frequency oscillations with dfig wind power generation," *IET Generation, Transmission & Distribution*, 2019.

[5] R. Shah, N. Mithulananthan, and K. Y. Lee, "Large-scale pv plant with a robust controller considering power oscillation damping," *IEEE Transactions on Energy Conversion*, vol. 28, no. 1, pp. 106–116, 2012.

[6] Y. Shen, W. Yao, J. Wen, and H. He, "Adaptive wide-area power oscillation damper design for photovoltaic plant considering delay compensation," *IET Generation, Transmission & Distribution*, vol. 11, no. 18, pp. 4511–4519, 2017.

[7] D. Remon, A. M. Cantarellas, J. M. Mauricio, and P. Rodriguez, "Power system stability analysis under increasing penetration of photovoltaic power plants with synchronous power controllers," *IET Renewable Power Generation*, vol. 11, no. 6, pp. 733–741, 2017.

[8] L. Zhou, X. Yu, B. Li, C. Zheng, J. Liu, Q. Liu, and K. Guo, "Damping inter-area oscillations with large-scale pv plant by modified multiple-model adaptive control strategy," *IEEE Transactions on Sustainable Energy*, vol. 8, no. 4, pp. 1629–1636, 2017.

[9] L. Wang, Q.-S. Vo, and A. V. Prokhorov, "Stability improvement of a multimachine power system connected with a large-scale hybrid wind-photovoltaic farm using a supercapacitor," *IEEE Transactions on Industry Applications*, vol. 54, no. 1, pp. 50–60, 2017.

[10] S. R. Paital, P. K. Ray, A. Mohanty, and S. Dash, "Stability improvement in solar pv integrated power system using quasi-differential search optimized svc controller," *Optik*, vol. 170, pp. 420–430, 2018.

[11] M. Darabian, A. Jalilvand, and M. Azari, "Power system stability enhancement in the presence of renewable energy resources and hvdc lines based on predictive control strategy," *International Journal of Electrical Power & Energy Systems*, vol. 80, pp. 363–373, 2016.

[12] R. Shah, N. Mithulananathan, and K. Y. Lee, "Design of robust power oscillation damping controller for large-scale pv plant," in *2012 IEEE Power and Energy Society General Meeting*. IEEE, 2012, pp. 1–8.

[13] Y. Wang and L. Xu, "Coordinated control of dfig and fsig-based wind farms under unbalanced grid conditions," *IEEE Transactions on Power Delivery*, vol. 25, no. 1, pp. 367–377, 2010.

[14] P. W. Sauer and M. Pai, "Power system dynamics and stability," *Urbana*, 1998.

[15] I. Hiskens, "Ieee pes task force on benchmark systems for stability controls," *Technical Report*, 2013.

[16] M. G. Villalva, J. R. Gazoli, and E. Ruppert Filho, "Modeling and circuit-based simulation of photovoltaic arrays," in *2009 Brazilian Power Electronics Conference*. IEEE, 2009, pp. 1244–1254.

[17] K. Zhou and J. C. Doyle, *Essentials of robust control*. Prentice hall Upper Saddle River, NJ, 1998, vol. 104.

[18] P. Gahinet, A. Nemirovskii, A. J. Laub, and M. Chilali, "The lmi control toolbox," in *Decision and Control, 1994., Proceedings of the 33rd IEEE Conference on*, vol. 3. IEEE, 1994, pp. 2038–2041.